J Wood Sci (2011) 57:195–202
DOI 10.1007/s10086-010-1159-5


ORIGINAL ARTICLE

**Sung-Jun Pang · Jung-Kwon Oh · Chun-Young Park**
**Jun-Jae Lee**

# Influence of crossing-beam shoulder and wood species on moment-carrying capacity in a Korean traditional dovetail joint

Received: June 7, 2010 / Accepted: October 3, 2010 / Published online: February 25, 2011

**Abstract** This study investigated the interaction effects of a crossing beam on the moment-carrying capacity of a Korean traditional dovetail joint. In particular, the length of the crossing-beam shoulder ($B_s$) and the wood species were varied as important factors. Clearly, the $B_s$ acts as a fastener that improves the performance of timber joints by preventing splitting failure parallel to the grain. All the specimens experienced tension failure by tension force in the direction perpendicular to the grain; therefore, the tension strength perpendicular to the grain could be considered an important property, and standard values could be determined to develop a formula for predicting the structural behavior of the joints or the structural design codes of the joints. The results of the tests indicated that the moment resistance of the joints increased as the length of the crossing $B_s$ and the density of the wood species increased. Joint stiffness results also indicated that the joints became stiffer when the crossing beam had shoulders, but the results were not affected by the length of the $B_s$. In addition, the joint stiffness was proportional to the density of the wood species.

**Key words** Traditional wooden Korean building · Traditional post–beam joint · Wood-to-wood joint · Dovetail joint · Mortise-and-tenon joint · Moment-carrying capacity · Beam shoulder ($B_s$) · Wood species

## Introduction

Hanok is the traditional Korean wooden building style, and the Korean government recently tried to industrialize and globalize it with the goal of adding value, boosting the national image, and incorporating traditional cultural elements into everyday lives. Traditional wooden buildings have been constructed based on empirical experience and craftsmanship. The fact that timber has been used as a building material for a long time does not mean that the behavior of the material is scientifically understood. At present, no rational design methods exist pertaining to the engineering of traditional timber frames.

Dovetail joints are commonly used at post–beam joints in traditional Korean wooden buildings. Post–beam joints are critical elements in the analysis of structural behavior. Several researchers[1–6] have tested the structural performance of the traditional joints, but the behavior of the joint and the factors that affect its performance are still not sufficiently understood. To develop rational design methods, it is foremost necessary to identify the factors that have significant impacts on the joints.

In the upper part of a post, the Korean traditional post–beam joints are composed of three members: post, beam, and *dori* (in Korean), which crosses through the beam. Each of the members is oriented in different directions and jointed on the top of the post (Fig. 1). Pang et al.[8] investigated the interaction effect of crossing members on the post–beam joints and discovered the effect of the beam shoulder ($B_s$), but they simply presented the joint performance with or without the $B_s$. However, not only did the size of the beam shoulder vary according to the builder, but also the joint was commonly made of wood from various species, e.g., Korean red pine (*Pinus densiflora*), Korean pine (*Pinus koraiensis*), and Japanese larch (*Larix kaempferi*). Therefore, to determine an efficient design method, the relationship between the $B_s$ and the joint performance should be ascertained, and the effect of species should be investigated. The study to find the optimized size of the beam shoulder will contribute to the development of standardized sizes for use in modernizing and industrializing Korean traditional wooden joints. The purpose of this study was to investigate the effect of wood density and to discover the relationship between the length of $B_s$ and the moment-carrying capacity in the Korean traditional dovetail joint.

S.-J. Pang · J.-K. Oh · J.-J. Lee (✉)
Department of Forest Sciences, Research Institute for Agriculture and Life Sciences, Seoul National University, Seoul 151-742, Korea
Tel. +82-2-880-4792; Fax +82-2-873-2318
e-mail: junjae@snu.ac.kr

C.-Y. Park
Department of Forest Sciences, Seoul National University, Seoul 151-742, Korea

## Materials and methods

### Specimens

Seven groups of dovetail joints, with three replications of each, were manufactured using Japanese cedar (*Cryptomeria japonica*, oven-dry density: 353 kg/m$^3$), Douglas fir (*Pseudotsuga menziesii*, oven-dry density: 427 kg/m$^3$), and Japanese larch (*Larix kaempferi*, oven-dry density: 478 kg/m$^3$) in air-dried conditions (moisture content: 12%–20%).

To identify the test specimens, joint IDs were established according to the species of wood, the post width ($P_w$), and the beam width ($B_w$), as shown in Fig. 2. For example, the joint ID C-180-60 in Table 1 indicates that the species of the joint is Japanese cedar, the $P_w$ is 180 mm, and the $B_w$ is 60 mm. A joint ID of C-180-180 means that the wood species and $P_w$ are the same as for C-180-60, and $B_w$ is 180 mm, so that the mortise branches are fully covered by the $B_s$.

Figure 3 shows how the three members are combined on top of a post; Figs 3a,b show the configuration of the dovetail joint before and after combining the three members, respectively. As shown in Fig. 3c, the $B_w$ of C-180-60 was 60 mm, and the specimen did not have a $B_s$ (0 mm). In contrast, the $B_w$ of C-180-180 was 180 mm, and the $B_s$ (60 mm) fully covered the mortise branches. As the $B_w$ increases in increments of 30 mm (such as C-180-90, C-180-120, and C-180-150), the $B_s$ increases in increments of 15 mm. In other words, the ratios of the length of the $B_s$ in joint configurations from C-180-60 to C-180-180 are 0:0.25:0.5:0.75:1.

To determine the influence of the $B_s$, $B_w$ alone was changed while the other dimensions of the beam, post, and *dori* were kept the same (Fig. 4). Regarding the size of the dovetailed tenon on the *dori*, the length of the tenon was the same as the length of the mortise branch on the post, the neck of the tenon was one-third of the *dori* width (180 mm), and the head of the tenon was 1.5 times larger than its neck. Therefore, the angle of the dovetailed tenon ($\alpha$) was approximately 1.32 radians according to Eq. 1. In addition, both the depth of the dovetailed tenon and the beam depth were the same as the *dori* depth.

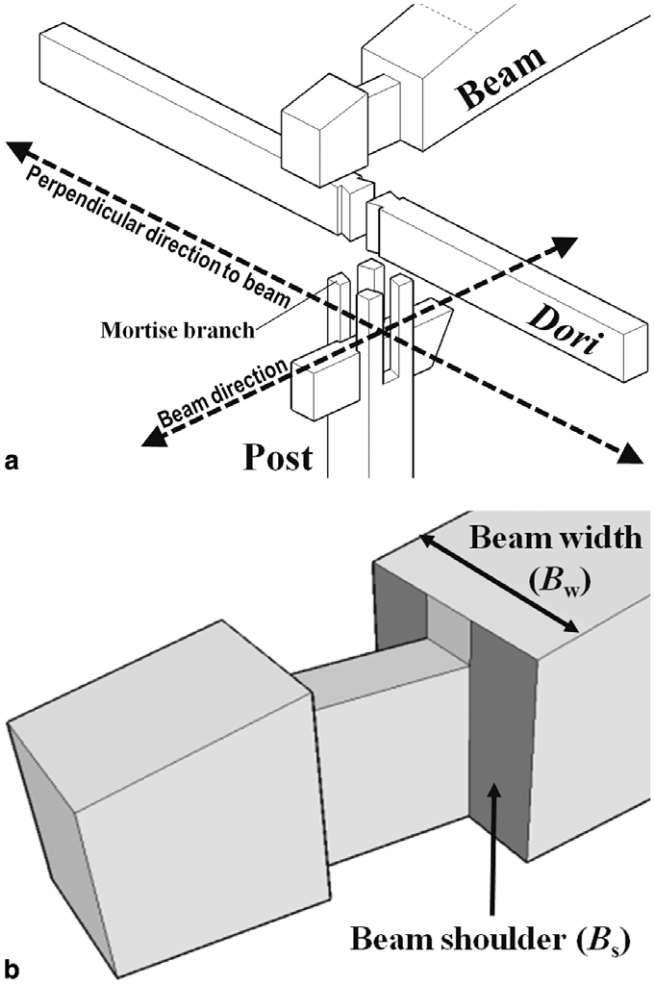


**Fig. 1a–b.** Korean traditional dovetail joint.[7] **a** Two members, the beam and *dori*, are jointed on top of the post; **b** the contact surface between beam shoulders and mortise branches of the post increases as the beam width increases

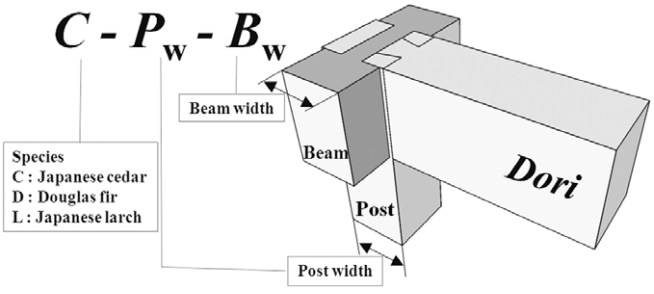


**Fig. 2.** The joint ID for test specimens is made up of a species identifier, the post width, and the beam width

**Table 1.** Ratios of moment-carrying capacity depending on the beam shoulder length

| | Joint ID | $L_{Bs}$ (mm) | $M_{max}$ (kN·m) | | $M_y$ (kN·m) | | $K_i$ (kN·m/rad.) | | Failure mode |
|---|---|---|---|---|---|---|---|---|---|
| | | | Average | $R_e$ | Average | $R_e$ | Average | $R_e$ | |
| a | C-180-60 | 0 | 0.75 | 0.31 | 0.41 | 0.28 | 5.08 | 0.45 | Top of the post |
| b | C-180-90 | 15 | 1.56 | 0.65 | 0.90 | 0.62 | 10.63 | 0.94 | Mortise branch |
| c | C-180-120 | 30 | 1.86 | 0.77 | 1.27 | 0.87 | 12.78 | 1.13 | Mortise branch |
| d | C-180-150 | 45 | 2.04 | 0.85 | 1.24 | 0.86 | 16.65 | 1.48 | Beam shoulder |
| e | C-180-180 | 60 | 2.40 | 1.00 | 1.45 | 1.00 | 11.26 | 1.00 | Beam shoulder |

$L_{Bs}$, the length of beam shoulder; $M_{max}$, maximum moment; $M_y$, yield moment; $K_i$, initial stiffness; $R_e$, the ratio of a, b, c, and d to e

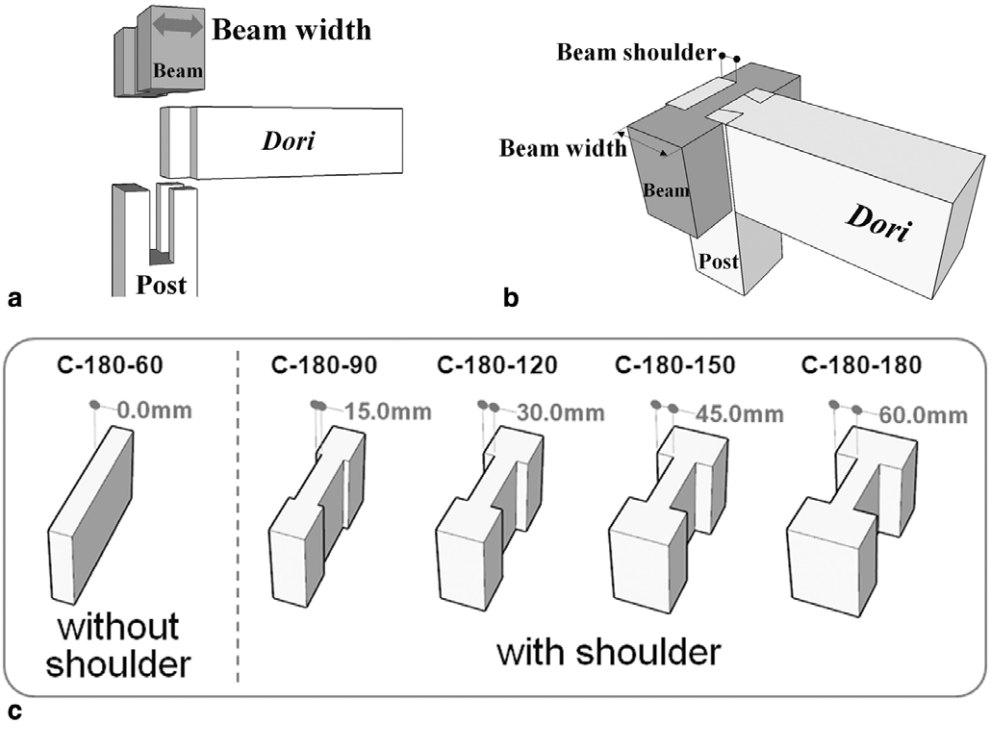


**Fig. 3a–c.** The configuration of a dovetail joint. **a** Before combining the members; **b** after combining the members; **c** the length of the beam shoulder in each specimen

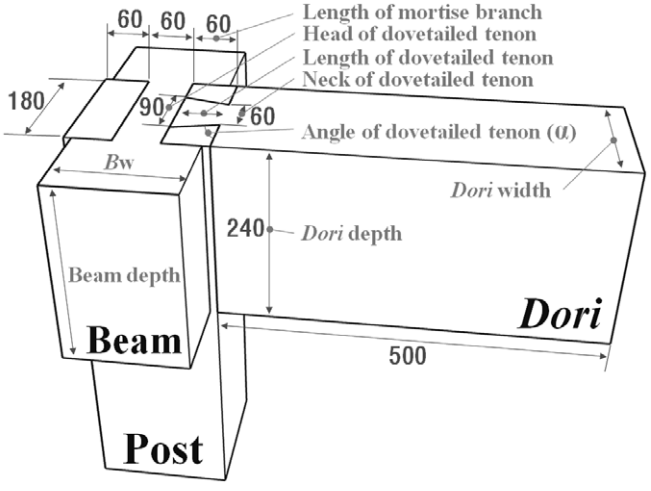


**Fig. 4.** The dimensions of specimens for testing the effect of the beam shoulder. Only the beam width ($B_w$) was changed, the other dimensions of the beam and both the post and *dori* were controlled with uniform shape and size

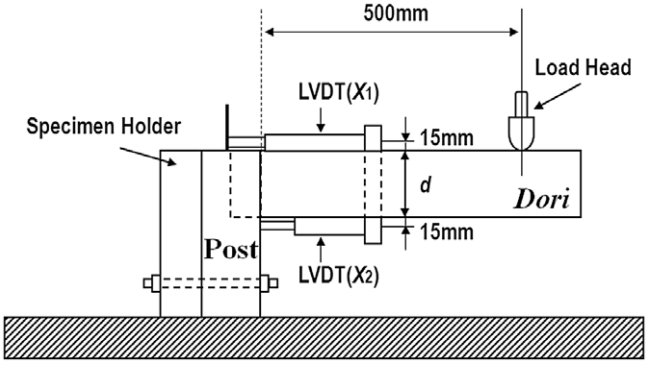


**Fig. 5.** Diagram of the setup used to test the specimens.[9] *LVDT*, linear variable differential transformer

$$\alpha = \arctan[L/\{(H-N)/2\}] \quad (1)$$

where $\alpha$ is the angle of the dovetailed tenon, $L$ is the length of dovetailed tenon (60 mm), $H$ is the head of dovetailed tenon (90 mm), $N$ is the neck of dovetailed tenon (60 mm).

## Experimental procedures

In order to investigate the moment–rotation characteristics and failure modes of dovetail joints, specimens were supported in a universal testing machine (Zwick) by means of the jig shown in Figs. 5 and 6. The load head speed was 5 mm/min. Measurements of joint flexibility were obtained by means of a linear variable differential transformer (LVDT) placed on the top edge of the *dori*. Testing continued until the applied load stopped increasing or until the occurrence of an obvious joint failure with a sudden falloff in load.

The internal joint rotation angle ($\theta$) was calculated using the displacement of both LVDT ($x_1$) and LVDT ($x_2$), as well as the distance between LVDT ($x_1$) and LVDT ($x_2$). By the geometric relationship between the joint rotation angle and displacements, as shown in Fig. 7, Eq. 2 can be obtained:

$$\theta = \arctan[(X_1 + X_2)/(15 + d + 15)] \quad (2)$$

where $X_1$ is the displacement of LVDT ($x_1$), measured on the top side of the *dori*; $X_2$ is the displacement of LVDT

**Fig. 6.** Test setup for evaluating the moment-carrying capacity of dovetail joints

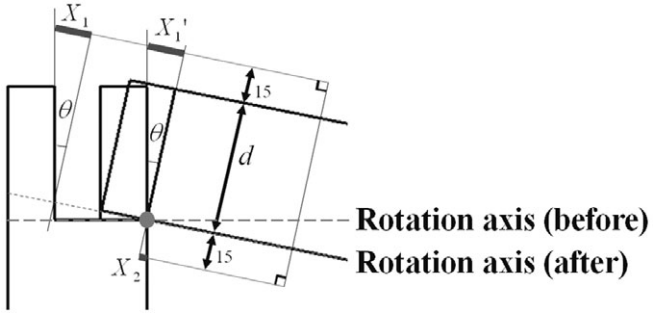


**Fig. 7.** Geometric relationship between joint rotation angle and displacement

($x_2$), measured on the bottom side of the *dori*; and 15 + $d$ + 15 is the distance between the two LVDTs, where $d$ is the depth of the *dori*.

Definition of the strength properties of the joints

The definitions and a method for calculating the strength properties of mechanical timber joints are shown in Fig. 8. The calculation was performed as follows:[10–12]

1. Line I, a straight line that connects 0.1 $M_{max}$ and 0.4 $M_{max}$ in the moment–deflection angle curve (where $M_{max}$ denotes the maximum moment), was drawn.
2. Line II, a straight line that connects 0.4 $M_{max}$ and 0.9 $M_{max}$ in the curve, was drawn.
3. Line II was offset in the $x$-axis direction in order to create a line tangent to the curve. This new line was defined as line III.
4. The moment corresponding to the intersection of lines I and III was defined as the yield moment ($M_y$). Line IV was drawn parallel to the $x$-axis through this point.
5. The deflection angle corresponding to the intersection of line IV and the curve was defined as the yield deflection angle ($\theta_y$).

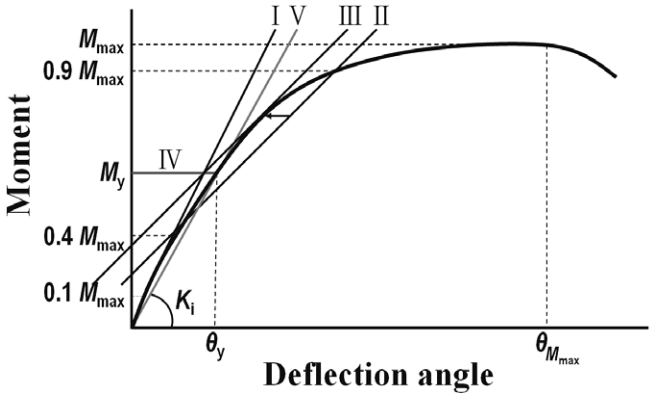


**Fig. 8.** Definition of the joint's performance. $M_{max}$, maximum moment; $M_y$, yield moment; $K_i$, initial stiffness; $\theta_y$, yield angle; $\theta_{Mmax}$, deflection angle at maximum moment. The determination of *lines I–V* is given in the text

6. Line V, the straight line that connects the origin and the coordinates ($M_y$, $\theta_y$) was drawn. The slope of this line was defined as the initial stiffness ($K_i$) and was calculated using Eq. 3:

$$\text{Initial stiffness } (K_i) = M_y/\theta_y \text{ (kN·m/rad.)} \quad (3)$$

## Results and discussion

Influence of beam shoulder on failure modes

The failure modes of the specimens in this test differed depending on the length of the $B_s$ and $B_w$, as shown in Fig. 9. For specimens without a $B_s$ (C-180-60, $B_w$: 60, length of $B_s$: 0 mm), the gap between the mortise branches widened as the moment increased, as shown in Fig. 9a, and tension failures occurred on top of the post, as shown in Fig. 9b. However, for specimens with a $B_s$, shear failures of the mortise branches (C-180-90 and C-180-120) or tension failures of the $B_s$ (C-180-150 and C-180-180) occurred. It can be considered that the presence of a $B_s$ prevented mortise branches from moving outward and resulted in the different failure modes.

Joint rotation occurred due to the vertical load (F), as shown in Fig. 10a, and the mortise branch moved outward by the angle of the dovetailed tenon ($\alpha$), as shown in Fig. 10b. This mechanism appeared in the case of specimens without a $B_s$ and the behavior of the mortise branch caused a tension force perpendicular to the grain on the post, and the tension failure was checked on top of the post. In the case of specimens with a $B_s$, when the length of the $B_s$ was 15–30 mm, the $B_s$ prevented this behavior of the mortise branches. As the movement of the mortise branches was prevented, friction occurred between the dovetailed tenon and mortise branches, and rolling shear failures appeared at the mortise branches due to shear force between the dovetailed tenon and $B_s$, as shown in Fig. 10c. When the length of the $B_s$ was increased to 45–60 mm, tension failures occurred at the $B_s$ on the beam instead of rolling shear

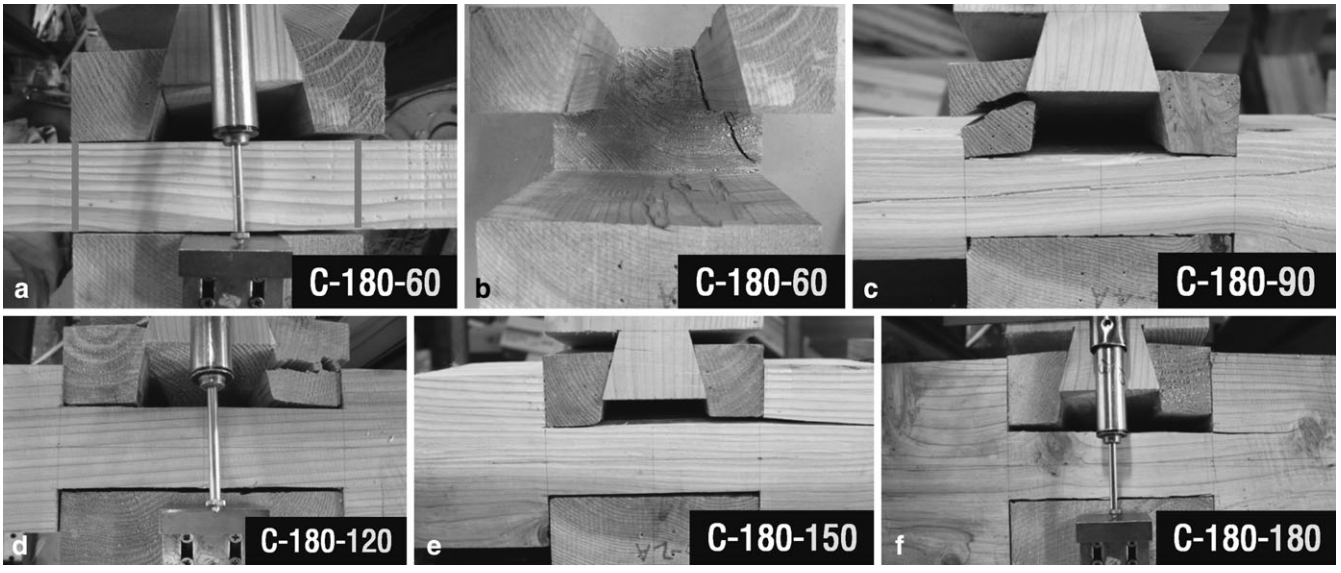


**Fig. 9a–f.** Failure modes of dovetail joints in the test. **a** The mortise branch moves outward; **b** split failure parallel to the grain at the post; **c,d** rolling shear failure at the mortise branch; **e,f** split failure parallel to the grain at the beam shoulder on the beam

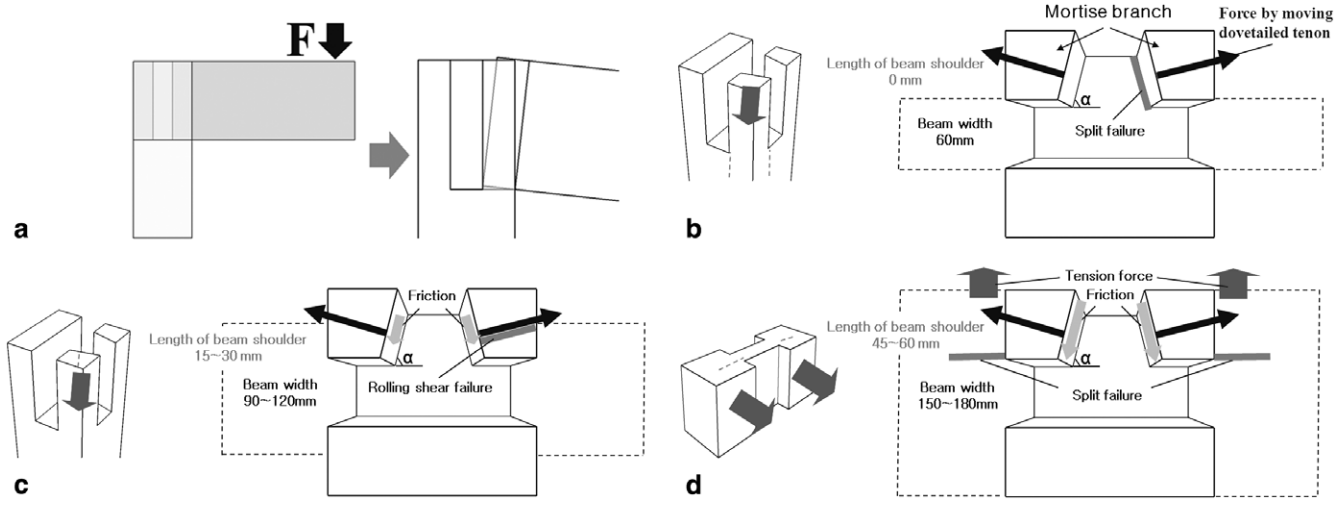


**Fig. 10a–d.** Diagrams of failure modes depending on the length of the beam shoulder. **a** Behavior of the dovetail joint; **b** split failure parallel to the grain at the post, where $\alpha$ is the angle of the dovetailed tenon; **c** rolling shear failure parallel to the grain at the mortise branch; **d** split failure parallel to the grain at the beam shoulder on the beam

failure at the mortise branches. As both mortise branches moved outward, the $B_s$ also moved outward with the mortise branches, and a tension force occurred at the $B_s$ on the beam, as shown in Fig. 10d.

The phenomena in which the different failure modes occur can be explained by friction as shown in Fig. 11, and the friction can be expressed as Coulomb friction as follows:

$$F_n \leq \mu N_n \tag{4}$$

where $F_n$ is the force exerted by friction; $\mu$ is the coefficient of friction, which is an empirical property of the contacting materials; and $N_n$ is the normal force exerted between the surfaces.

When a $B_s$ is present, frictional forces $F_{Bs}$ (between $B_s$ and the mortise branch) and $F_{Mb}$ (between the mortise

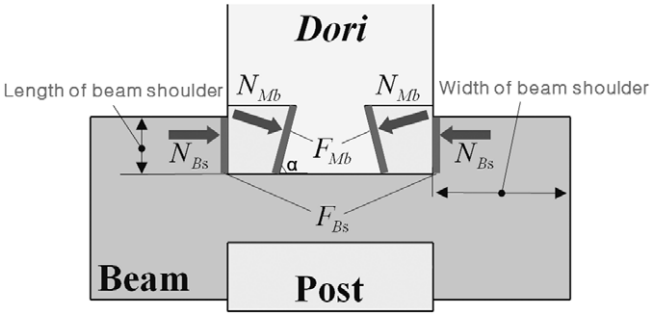


**Fig. 11.** Friction diagram. $N_{Bs}$, normal force between beam shoulder and mortise branch; $N_{Mb}$, normal force between mortise branch and dovetailed tenon; $F_{Bs}$, frictional force between beam shoulder and mortise branch; $F_{Mb}$, frictional force between mortise branch and dovetailed tenon

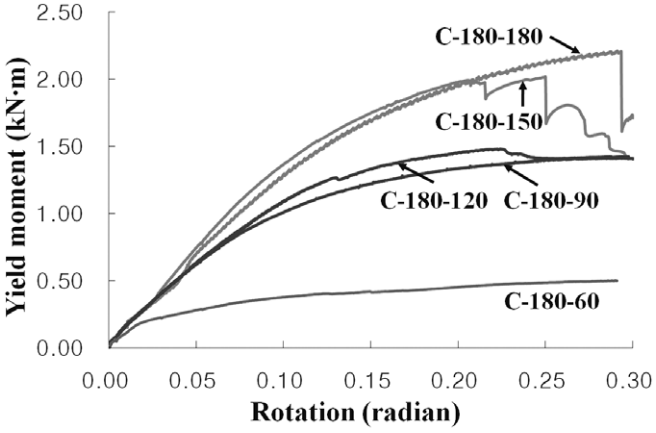


**Fig. 12.** The moment–rotation curve. C-180-60, split failure occurred at the post; C-180-90 and C-180-120, rolling shear failure occurred at the mortise branch; C-180-150 and C-180-180, split failure occurred at the beam shoulder on the beam

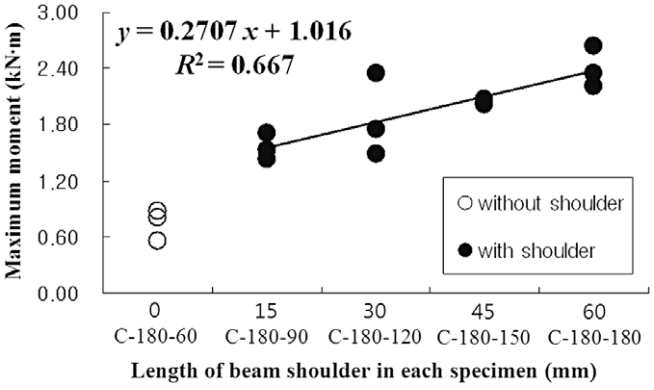


**Fig. 13.** Relationship between the length of the beam shoulder ($B_s$) and the maximum moment ($M_{max}$)

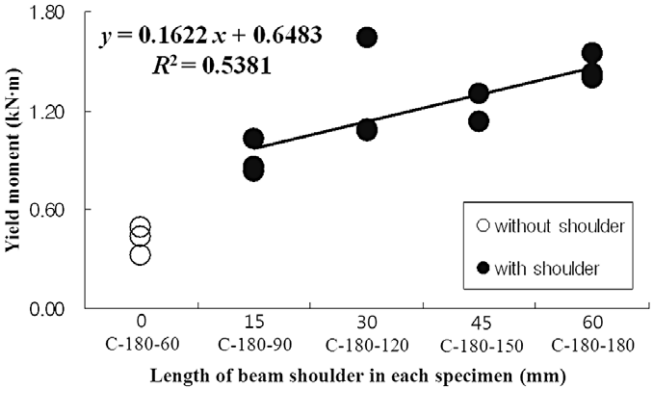


**Fig. 14.** Relationship between the length of the $B_s$ and the yield moment ($M_y$)

branch and dovetailed tenon on the *dori*) occur due to the length of $B_s$ and the normal forces $N_{Bs}$ (between $B_s$ and the mortise branch) and $N_{Mb}$ (between the mortise branch and dovetailed tenon on the *dori*), perpendicular to the surface of contact. The contact surfaces between the $B_s$ and the mortise branch increase as the length of $B_s$ increases, and the normal forces ($N_{Bs}$ and $N_{Mb}$) also increase because the movement of the mortise branches is prevented by the $B_s$.

If movement of the dovetailed tenon causes $N_{Mb}$ to exceed the rolling shear resistance of the mortise branch, then rolling shear failure appears, as shown in Fig. 10c. If the $B_s$ (Fig. 11) is not sufficiently wide and $N_{Bs}$ is greater than the shear resistance of the $B_s$ on the beam, then shear failure appears in the $B_s$ on the beam instead of split failure caused by the tension force. In this study, the width of the $B_s$ was 120 mm and shear failure of the $B_s$ did not occur; however, both the width and length of the $B_s$ are important to consider.

As a result, the $B_s$ acts as a fastener[13–15] that improves the performance of timber joints by preventing splitting failure parallel to the grain. In addition, the friction between the dovetailed tenon and mortise branches increases as the length of the $B_s$ increases.

## Influence of beam shoulder on moment-carrying capacity

The moment–rotation curves (Fig. 12) show that the effect of the $B_s$ was also evident in the moment capacity and the initial stiffness. Both the moment capacity and the initial stiffness varied depending on the absence or presence of a $B_s$. In addition, for joints with a $B_s$, the maximum moment ($M_{max}$) increased as the length of the $B_s$ increased (Fig. 13), and the yield moment ($M_y$) also tended to increase as the length of the $B_s$ increased (Fig. 14). The tendency of the moment also increased, depending on the length of the $B_s$. The relationship between $M_{max}$ and the length of the $B_s$ was similar to that between $M_y$ and the length of the $B_s$. Therefore, the yield moment depends on the maximum moment and the failure modes related to the maximum moment.

The difference in mechanical properties depending on the length of the $B_s$ seems to be caused by friction affecting the different failure modes, as shown in Fig. 11. In other words, the friction force increased due to the fixed mortise branches and this improved both the moment capacity and the initial stiffness. This means that the friction reinforced by the $B_s$ affects the failure modes and increases the moment capacity.

The initial stiffness ($K_i$) also varied depending on the absence or presence of the $B_s$. However, in the presence of a $B_s$, initial stiffness did not tend to increase as the length of the $B_s$ increased, as shown in Fig. 15. However, the maximum and yield moments tended to increase as the length of the $B_s$ increased. The initial stiffness was affected by the absence or presence of a $B_s$, but was not affected by its length.

Table 1 shows the properties, the maximum moment ($M_{max}$), the yield moment ($M_y$), and the initial stiffness ($K_i$) values of each specimen. $R_e$ values represent the ratios of the values of each specimen to those of C-180-180, in which the mortise branches are fully covered by the $B_s$. For example, the $M_{max}$ values of C-180-60 specimens (without a $B_s$) averaged 31% of the corresponding values of C-180-180

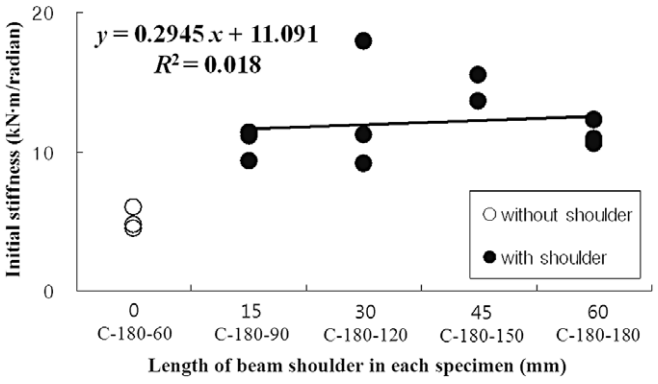


**Fig. 15.** Relationship between the length of the $B_s$ and the initial stiffness ($K_i$)

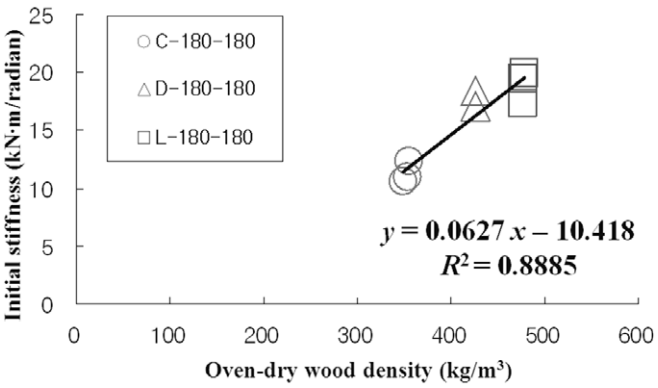


**Fig. 16.** Relationship between wood density and initial stiffness ($K_i$)

specimens, and $M_y$ values were approximately 28% those of C-180-180. The ratios of $M_{max}$ and $M_y$ for joints increased as the length of the $B_s$ increased. Meanwhile, although the average $K_i$ of C-180-60 was about 45% that of C-180-180, the average $K_i$ for C-180-90 (which has a $B_s$ length of 15 mm) averaged 94% that of C-180-180. When the length of the $B_s$ was 30 or 45 mm, the average $K_i$ exceeded the average $K_i$ of C-180-180. Therefore, the $K_i$ of specimens with a $B_s$ was distinct from the specimens without a $B_s$, and the $K_i$ of dovetail joints could be reinforced by the $B_s$, even when a beam had a short $B_s$.

## Wood species versus mechanical properties of dovetail joints

The mortise branches of specimens used to investigate the effect of wood species were fully covered with the $B_s$ (i.e., $B_w$ was 180 mm), and the failure modes of specimens were the same regardless of species. All specimens failed at the $B_s$ on the beam, and tension failure by tension force perpendicular to the grain occurred, as shown in Figs. 9f and 10d.

The effect of density with respect to species was clarified in the relationship with joint stiffness and moment capacity. Density was measured at the part nearest to the failure. Initial stiffness ($K_i$) was proportional to the density, as shown in Fig. 16. The maximum moment ($M_{max}$) and yield moment ($M_y$) were also proportional to the density, as shown in Figs. 17 and 18. However, the gradients of the density–$M_{max}$ and density–$M_y$ relationships were lower than the gradient of the density–$K_i$ relationship.

It could be considered that the moment capacity was influenced by the failures. Moment capacity is clearly closely related to failures, and so tension failures by tenson force perpendicular to the grain were investigated. In fact, tension strength perpendicular to the grain is highly related to the cleavage strength, which is the lowest strength property of wood, as well as having the lowest difference between species of any property according to data from previous studies.[16–18] As a result, it seems that the $M_{max}$ and $M_y$ values were less influenced than the $K_i$ values were by the wood density, due to the cleavage resistance.

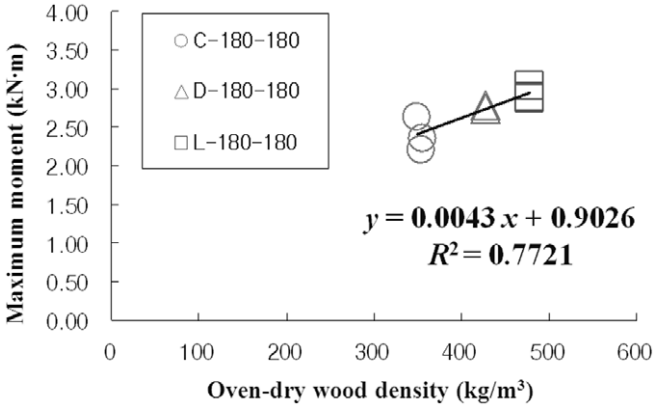


**Fig. 17.** Relationship between wood density and maximum moment ($M_{max}$)

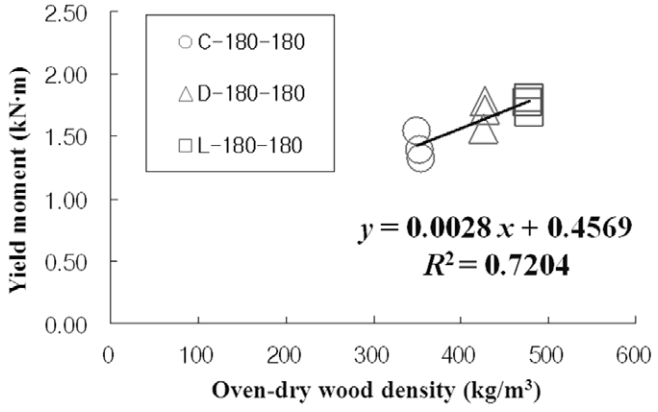


**Fig. 18.** Relationship between wood density and yield moment ($M_y$)

In Table 2, $R_c$ shows the ratios of the properties for each specimen to those of L-180-180 (Japanese larch) specimens. C-180-180 (Japanese cedar) joints had approximately 83% of the $M_y$ and 60% of the $K_i$ of Japanese larch. D-180-180 joints (Douglas fir) had about 96% of the $M_y$ and 93% of the $K_i$ of the equivalent joint made from Japanese larch. These results indicate that $K_i$ was more affected by the

**Table 2.** Ratios of moment-carrying capacity depending on wood species

| | Joint ID | Species | Oven-dry density (kg/m$^3$) | $M_{max}$ (kN·m) | | $M_y$ (kN·m) | | $K_i$ (kN·m/rad) | |
|---|---|---|---|---|---|---|---|---|---|
| | | | | Average | $R_c$ | Average | $R_c$ | Average | $R_c$ |
| a | C-180-180 | Japanese cedar | 353 | 2.40 | 0.82 | 1.45 | 0.83 | 11.26 | 0.60 |
| b | D-180-180 | Douglas fir | 427 | 2.76 | 0.94 | 1.69 | 0.96 | 17.45 | 0.93 |
| c | L-180-180 | Japanese larch | 478 | 2.94 | 1.00 | 1.76 | 1.00 | 18.86 | 1.00 |

$M_{max}$, maximum moment; $M_y$, yield moment; $K_i$, initial stiffness; $R_c$, the ratio of a and b to c

wood species than the other parameters were. Therefore, the wood species should be considered as a factor in the structural design of a dovetail joint.

## Conclusions

The experimental results regarding failure modes and moment resistance indicated that the length of the $B_s$ and the wood species significantly affected the performance of Korean traditional dovetail joints; it was clear that the $B_s$ acts as a fastener that improves the performance of timber joints by preventing splitting failure parallel to the grain.

For all failure modes, the failures occurred by tension force perpendicular to the grain. Therefore, the tension strength perpendicular to the grain is an important property and can be determined as standard values to develop a formula for predicting the structural behavior of the joints or the structural design codes of the joints.

The moment resistance of the joints was affected by the $B_s$ length and became higher as the length increased. Joint stiffness results also indicated that the joints stiffened when the beam had a $B_s$, but were not affected by its length. The joint stiffness and moment resistance were proportional to the density of the wood species, but the moment resistance tended to be less sensitive to the wood density than the joint stiffness was.

**Acknowledgments** This study was carried out with a grant from the Forest Science and Technology Projects (Project No. S120710L100110) funded by the Korean Forest Service.

## References

1. Chang WS, Shanks J, Kitamori A, Komatsu K (2009) The structural behaviour of timber joints subjected to bi-axial bending. Earthq Eng Struct Dyn 38:739–757
2. Han SR, Lee JJ (2006) Mechanical performance of Korean traditional wooden building of the column-girder tenon-joint by joint type. In: Proceedings of the 9th world conference on timber engineering. August 6–10, 2006, Portland, OR, USA, p 294
3. Nakao M, Gotou M, Suzuki Y (2010) Experimental study on pull-out strength of mortise-tenon joint with pin subjected to bending moment. In: Proceedings of the 11th world conference on timber engineering. June 2–5, 2008, Miyazaki, Japan, pp 303–304
4. Seo JM, Choi IK, Lee JR (1999) Static and cyclic behavior of wooden frames with tenon joints under lateral load. J Struct Eng ASCE 125:344–349
5. Shim KB, Park JS, Yeo HM, Kim YI, Han JS (2006) Modernization of traditional Korean building systems with engineering methods. In: Proceedings of the 9th world conference on timber engineering. August 6–10, 2006, Portland, OR, USA, p 246
6. Shiratori T, Leijten AJM, Komatsu K (2009) The structural behaviour of a pre-stressed column-beam connection as an alternative to the traditional timber joint system. Eng Struct 31:2526–2533
7. Kim YS, Song IH (2005) Research on the construction method of the upper part of the post in traditional urban housing in Bukchon, Seoul (in Korean). J Archit Inst Korea 21:171–178
8. Pang SJ, Oh JK, Park JS, Park CY, Lee JJ (2010) Moment-carrying capacity of dovetailed mortise and tenon joints with or without beam shoulder. J Struct Eng ASCE. doi: 10.1061/(ASCE)ST.1943-541X.0000323
9. Erdil YZ, Kasal A, Eckelman CA (2005) Bending moment capacity of rectangular mortise and tenon furniture joints. Forest Prod J 55:209–213
10. Harada M, Hayashi Y, Hayashi T, Karube M, Ohgama T (2005) Effect of moisture content of members on mechanical properties of timber joints. J Wood Sci 51:282–285
11. Japan 2 × 4 Home Builders Association (2002) Structural design guidelines for wood frame construction (in Japanese). Japan 2 × 4 Home Builders Association, Tokyo, pp 239–240
12. Yasumura M, Kawai N (1997) Evaluation of wood-framed shear walls subjected to lateral load. Proceedings of the 30th CIB-W18. August 25–28, Vancouver, Canada, Paper 30-15-4
13. Thelandersson S (2003) Timber engineering. Wiley, Chichester, pp 323–324
14. Jonsson J (2005) Load carrying capacity of curved glulam beams reinforced with self-tapping screws. Holz als Roh- und Werkstoff 63:342–346
15. Tannert T, Lam F (2009) Self-tapping screws as reinforcement for rounded dovetail connections. Struct Control Health Monit 16:374–384
16. Wangaard FF (1950) The mechanical properties of wood. Wiley, New York, pp 15–16
17. Kilic M, Celebi G (2006) Compression, cleavage, and shear resistance of composite construction materials produced from softwoods and hardwoods. J App Polym Sci 102:3673–3678
18. Erdil YZ, Kasal A, Zhang J, Efe H, Dizel T (2009) Comparison of mechanical properties of solid wood and laminated veneer lumber fabricated from Turkish beech, Scotch pine, and Lombardy poplar. Forest Prod J 59:55–60